Origin and extent of fresh groundwater, salty paleowaters and recent saltwater intrusions in Red River flood plain aquifers, Vietnam

Luu T. Tran · Flemming Larsen · Nhan Q. Pham · Anders V. Christiansen · Nghi Tran · Hung V. Vu · Long V. Tran · Hoan V. Hoang · Klaus Hinsby

Abstract A model has been established on the origin and extent of fresh groundwater, salty paleowaters and saltwater from recent seawater intrusions in the Red River flood plain in Vietnam. This was done with geological observations, geophysical borehole logging and transient electromagnetic methods. Salt paleowater is present up to 50–75km from the coastline, with occurrence controlled by the Holocene transgression. A density-driven leaching of salty porewater has occurred from high-permeability Holocene sediments into underlying Pleistocene deposits, whereas diffusion has dominated in low-permeability layers. In the Pleistocene aquifer, the highest content of dissolved solids is found below two intrinsic valleys with Holocene marine sediments and along the coastline. Recent intrusion of saltwater from the South China Sea is observed in shallow groundwater 35km inland, probably a result of transport of salty water inland in rivers or leaching of paleowaters from very young near-coast marine sediments. The observed inverted salinity profile, with high saline water overlying fresher groundwater, has been formed due to the global eustatic sea-level changes during the last 8,000–9,000years. The proposed model may therefore be applicable to other coastal aquifers, with a proper incorporation of the local geological environments.

Received: 14 June 2011 / Accepted: 16 May 2012

L. T. Tran · N. Q. Pham · H. V. Vu · L. V. Tran · H. V. Hoang
Hanoi University of Mining and Geology,
Dong Ngac, Tu Liem Dist, Hanoi, Vietnam

F. Larsen (✉) · A. V. Christiansen · K. Hinsby
Geological Survey of Denmark and Greenland,
10 Øster Voldgade, 1350 Copenhagen, Denmark
e-mail: flar@geus.dk
Tel.: +45-3814-2323
Fax: +45-3814-2050

N. Tran
Hanoi University of Science,
No. 334, Nguyen Trai Street, Thanh Xuan District, Hanoi, Vietnam

Keywords Salinization · Transient electromagnetic soundings (TEM) · Geophysical borehole logging · Groundwater/surface-water relations · Vietnam

Introduction

Delta areas with their adjacent coastal zones and flood plains are often highly populated with intense agricultural and industrial production activities. Generally, groundwater abstraction imposes a risk of saltwater intrusion in such hydrogeological settings. In addition salty paleowaters may also be present in aquitards, which may deteriorate the water quality. 'Paleowater' is here defined as groundwater formed under previous climatic conditions and hydrogeological settings (Edmunds 2001). A number of studies and reviews have been published during the last few decades that investigate the risks of groundwater resource deterioration due to saltwater intrusion or mixing with salty paleowater, e.g. from Europe (De Vries 1981; Kooi et al. 2000; Edmunds and Milne 2001; Lozano et al. 2002; Balia et al. 2003; Post and Kooi 2003a; Post et al. 2003b; Antonelli et al. 2008; Custodio 2010), Asia (Zengcui and Yaqin 1989; Cheng and Chen 2001; Radhakrisna 2001; Hiroshiro et al. 2006; Le and Song 2007), on Pacific islands (White and Falkland 2010), Africa (Khalil 2006; Akouvi et al. 2008; Gossel et al. 2010; Steyl and Dennis 2010), Australia (Zhang et al. 2004; Werner 2010), North America (Barlow and Reichard 2010) and South America (Bocanegra et al. 2010). The focus in this study is the Red River flood and delta plain (Bac Bo Plain) in Vietnam, where recent saltwater intrusion has occurred from the South China Sea, and salty paleowaters from Holocene marine sediments impose severe restrictions on the use of the groundwater resources.

The Red River delta and flood plain is located in the northern part of Vietnam (Fig. 1). This delta with its flood plain covers an area of 21,063 km^2 and is inhabited by a fast growing population, which in 2010 numbered 19.8 million people (General Statistic Office 2011). In the rural areas, the socio-economic activities are based on intensive agricultural production of mainly rice and vegetables, with an irrigation system based on surface water. In the urban areas, e.g. Hanoi and Haiphong, the growing population

DOI 10.1007/s10040-012-0874-y

Published online: 13 June 2012

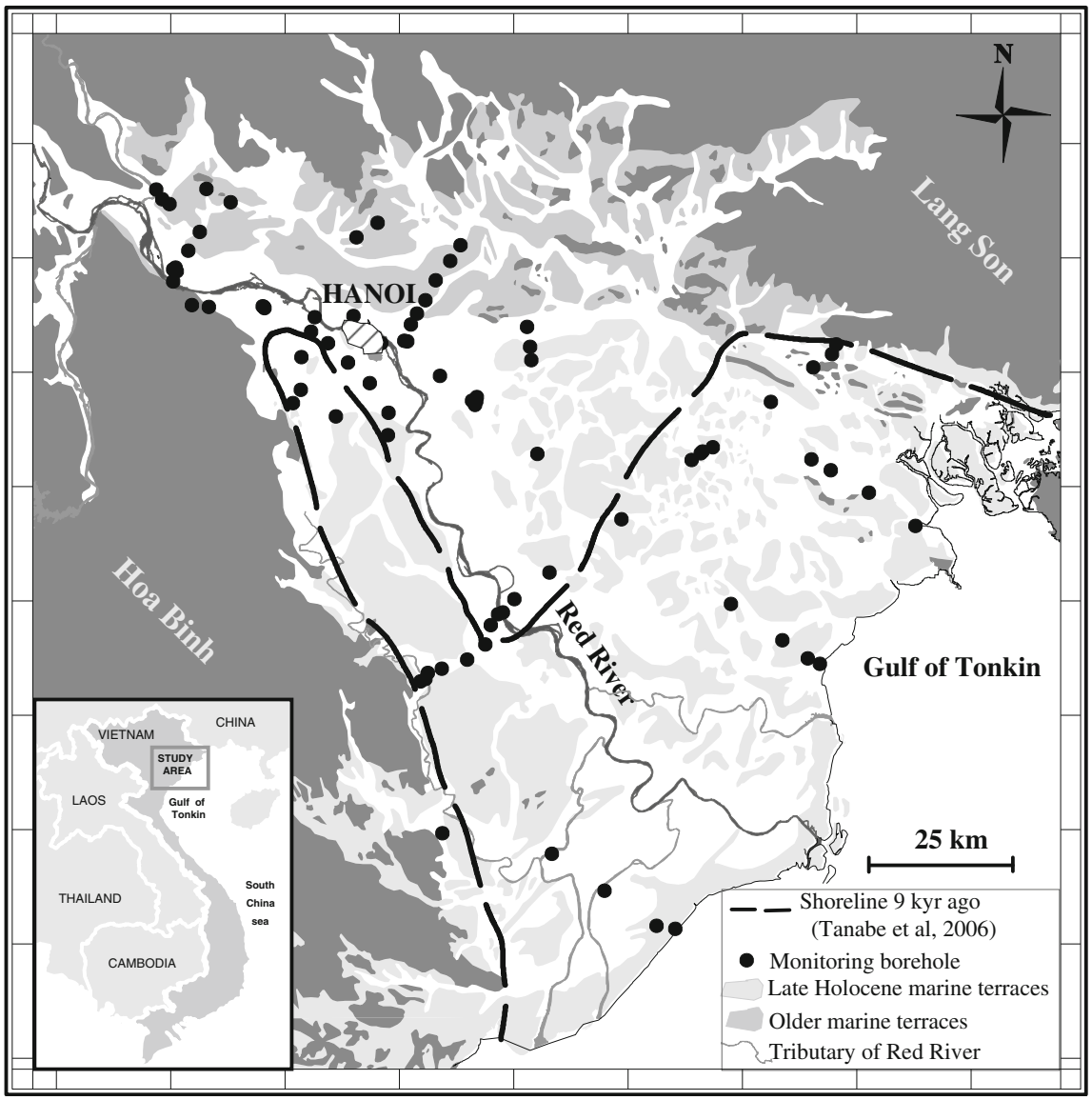

Fig. 1 The geography of the Red River flood plain and delta area, including locations of boreholes of the Vietnamese national groundwater monitoring network. The current extent of the marine terraces is from Hoang et al. 1998

and increasing industrial activities result in an increasing use of potable water, which in the Red River flood plain comes from groundwater abstraction. Even though the Red River flood plain cannot be characterized as a region of water scarcity, water-quality problems can locally lead to critical situations (Minh et al. 2010). The main groundwater quality problems are elevated concentrations of arsenic, manganese, ammonium and iron (Berg et al. 2001; Postma et al. 2007; Winkel et al. 2011) and the occurrence of salty groundwater (Pham 2000; Nguyen 2005; Jessen et al. 2008; Winkel et al. 2011). The flat and low lying Red River flood plain and coastal areas are vulnerable to saltwater intrusion, particular because of a relatively high subsidence rate in the area of 1 mm/yr (Tanabe et al. 2006) and curtailment of sediment supply due to the human construction of a system of dikes along the rivers, initiated 1,000 years (1 kyr) ago. Previous works have shown that salty groundwater is widespread and that it is occurring in the flood plain as far inland as 75 km from the coastline (Pham 2000; Nguyen 2005); concentrations of chloride as high as 10 g/L have been found in a zone up to 35 km from the coastline (Hoang et al. 2009). Therefore, although the distribution of salty groundwater in the Red River is more or less known, a clear understanding of the processes controlling the far inland occurrence of salty groundwater in the Red River flood plain has not yet been established.

The aim of this study is to establish a conceptual hydrogeological model for the origin and extent of fresh groundwater, salty paleowaters and recent saltwater intrusions in the Pleistocene and Holocene aquifers in the Red River flood plain. This is done through geophysical investigations along four survey lines in the flood plain, and the findings are presented in maps showing the distribution of the three defined water types in the Holocene and Pleistocene aquifers.

DOI 10.1007/s10040-012-0874-y

The geology and hydrogeology of the study area

The Red River flood plain makes up the northwestern part of the Song Hong Sedimentary Basin; a basin filled up with Palaeogene, Neogene and Quaternary sediments (Nielsen et al. 1999). The geographical extent of this sedimentary basin is limited by two NW–SE-striking converging faults that meet north of the capital Hanoi and control the course of the Red River into the Yunnan province in China (Rangin et al. 1995; Nielsen et al. 1999). The flood plain is surrounded by mountains composed of crystalline rocks from Paleozoic and Mesozoic sedimentary rocks (Mathers et al. 1996; Mathers and Zalasiewicz 1999).

The Quaternary geology of the Red River delta and flood plain has been summarized and studied by Tran et al. (1991); Mathers and Zalasiewicz (1999); Lam and Boyd (2003); Tanabe et al. (2003a, 2003b, 2006); Hori et al. (2004); Funabiki et al. (2007). The thickness of the Quaternary deposits ranges from a few meters in the flood plain apex in the NW to 150–200 m at the coastline in the SE. According to Tran et al. (1991), the sediments were deposited in five fining-upward sedimentary cycles. The first two of these cycles are of lower to middle Pleistocene age and are composed of coarse grained alluvial/fluvial deposits, followed by an upper Pleistocene cycle of fluvial deposits, which is grading upwards into deltaic-lacustrine-swamp environment sediments. The fourth cycle is of lower to middle Holocene age and is composed of fine-grained sands and clays formed in deltaic environments; the uppermost fifth cycle from the upper Holocene is dominated by coarse-grained deposits laid down in the delta plain and delta front environments.

The distribution and composition of late Pleistocene and Holocene sediments is overall controlled by variations in the eustatic sea-level changes in the South China Sea (Tanabe et al. 2006); from here on shortened to just 'sea-level changes'. The maximum regressive phase during the Quaternary period was in the middle to upper Pleistocene, and the maximum transgression was during the middle Holocene (Tran et al. 1991). The sea-level 20 kyr ago was about 120 m lower than the present sea-level, but increased gradually to its present level 8.5 kyr ago. From 6–4 kyr ago, the sea attained a highstand of 2–4 m above the present sea-level, and after this it gradually declined, reaching the present sea-level from 4 kyr to the present time (Fig. 2).

Schimanski and Stattegger (2005) used shallow high-resolution seismic profiles to document deep eroded structures into sediments on the northern shelf of Vietnam, formed during the low sea-level stands in the Pleistocene. On land an intrinsic valley, eroded with a depth of up to 80 m into the underlying Pleistocene deposits, has been identified on the west side of the present Red River (Tanabe et al. 2006; Funabiki et al. 2007). The location of this structure is indicated on Fig. 1 showing the interpreted shoreline 9 kyr ago. These erosion structures have subsequently been filled up with shallow marine sediments during the Holocene, beginning around 8.5 kyr ago, initiated by a deceleration in the sea-level rise at that time (Stanley and Warne 1994; Tanabe et al. 2006).

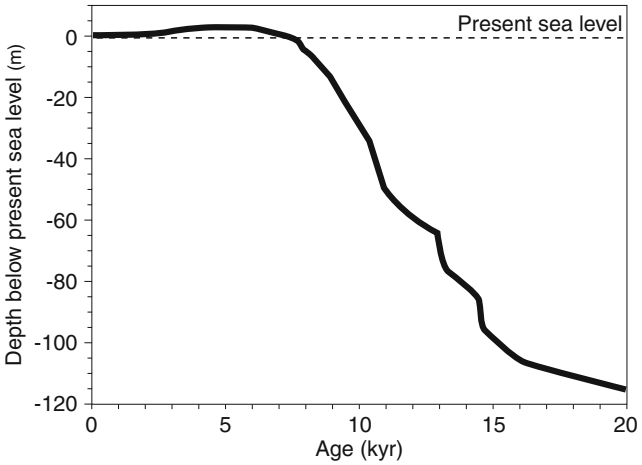

Fig. 2 Compiled eustatic sea-level curve for the western margin of the South China Sea during the past 20 kyr. (From Tanabe et al. 2006)

Near-surface layers with marine sediments dominated by fine sands and clays, so-called marine terraces, constitute a major part of the surface areas in the Red River flood plain (Fig. 1). During the Holocene, the sea transgressed the flood plain as far inland as the present location of Hanoi (Tanabe et al. 2006; Funabiki et al. 2007). The most inland Holocene marine terraces (Fig. 1) must have been deposited during the sea-level high stand from 6 to 4 kyr ago. The occurrence of older near-surface marine deposits, probably of lower or middle Pleistocene age, shows that the sea earlier in the Quaternary period must have submersed larger areas of the flood plain. Rivers have later eroded the marine terraces and subsequently deposited coarse-grained fluvial deposits and overbank fine grained deposits of silt and clay which here form the near-surface sediments. This distribution of Holocene marine sediments in the intrinsic valleys and the near-surface terraces has a paramount influence on the present distribution of salty groundwater in the flood-plain sediments.

The hydrological regime of the Red River flood plain has recently been studied by Minh et al. (2010). The flood plain is situated in the sub-tropical monsoon zone, with a rainy season from May–June to October–November. The mean annual precipitation in the period from 1996–2006 was 1,667 mm and 85 % of this is falling in the rain season. In a wet year (1996), the total discharge from the river system is around 140 km^3 (equal to 4,450 m^3/s) and in a dry year (2006) it reached 96 km^3 (equal to 3,100 m^3/s). The water stage in the Red River varies typically between 6 and 12 meter above sea-level (masl), reflecting the monsoon rainfall in the main catchment area in southern China and northern Vietnam. A pre-flooding season is seen with a fast increase in the river stage in May–June, the flooding takes place during July and August, and the post-flood season is from late August to October with a falling river stage.

The hydrogeology of the Red River flood plain aquifers is strongly influenced by an interaction with its many rivers and canals. During most of the year,

DOI 10.1007/s10040-012-0874-y

groundwater is discharging into the bodies of surface waters, but after the flooding the flow is reversed and surface water is recharging the aquifers (Larsen et al. 2008). The potential annual evapotranspiration has been estimated to be approximately 1,000 mm (Minh et al. 2010). The deeper Pleistocene aquifers are recharged by the surrounding mountain range and the average annual recharge to the aquifers is in the range of 100–400 mm. Hydraulic gradients in the range of 0.05–0.15 % are typical and groundwater flow velocities in the Holocene aquifers are a few tens of meters per year (Larsen et al. 2008).

Methodology

A national groundwater monitoring network was established in the Red River flood plain during the late 1990s, including 83 monitoring stations with separate boreholes screened in high-permeability Holocene and Pleistocene sediments. Most of these monitoring boreholes have been drilled along four lines throughout the flood plain, and these lines are used as survey lines in this study (Fig. 3). Each of the four survey lines includes a cross-section with geological information, and a profile with geophysical data.

Typically, two or three boreholes were drilled at each groundwater monitoring station and the shallow boreholes were equipped with OD 60-mm screens and deeper boreholes have OD 120-mm PVC casings and screens. The upper 60-mm screens are typically 6 m long, while the deepest screens are from 8 to 10 m in length. Lithological information from these boreholes has been used to describe the overall geology in the four survey lines.

As geophysical borehole logging can provide detailed and direct information on salinity and lithology variations

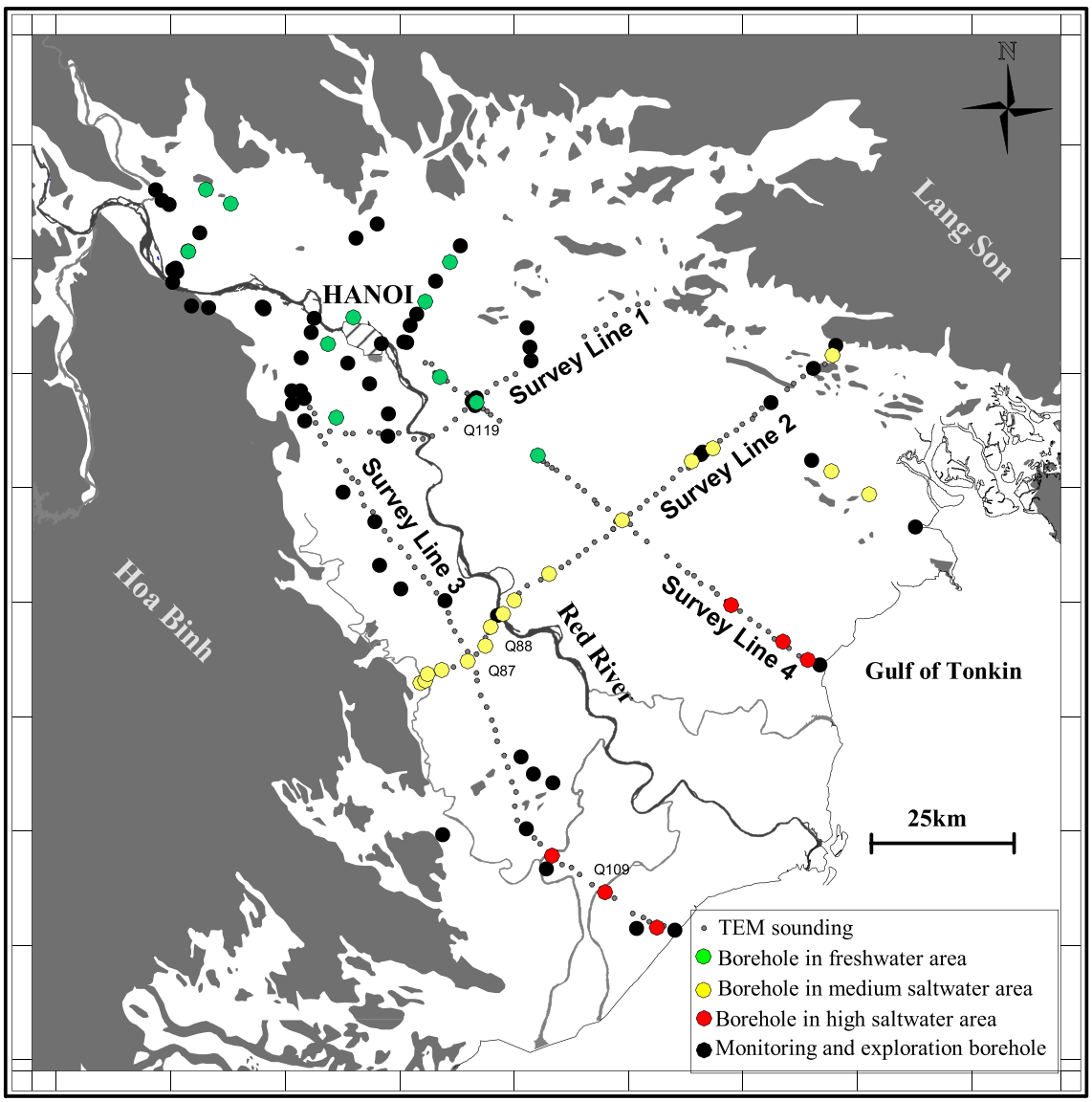

Fig. 3 Locations of the four survey lines with the 170 conducted TEM soundings in the Red River flood plain. Boreholes where geophysical logging was done are also indicated. *Green* boreholes are in areas with fresh groundwater. *Yellow* boreholes have medium saline groundwater and the *red* boreholes have high saline groundwater. For the definition of these water types see text

 DOI 10.1007/s10040-012-0874-y

at the wells (Buckley et al. 2001), logging was carried out in 38 of the national monitoring boreholes. Boreholes for these studies were selected to ensure a geographical coverage of the whole flood plain and expected variations in the subsurface geology. The location of the boreholes where geophysical logging was done is depicted in Fig. 3. Robinson Research Ltd equipment was used for the geophysical logging of the sediments for natural gamma radiation and formation electrical conductivities. Formation electrical conductivities were measured inside the PVC casings using a focussed induction probe, which has a formation penetration depth of around 5 m. Water electrical conductivity and temperature were also measured in the borehole, but these data are not shown here.

Formation electrical resistivities (ρ_f) from the borehole logging, expressed in ohm-m, were calculated from measured formation conductivity (σ_f), expressed in mS/m, using Eq. 1.

$$\rho_f \times \sigma_f = 1000 \quad (1)$$

Formation factors (F), given as the relationship between the formation electrical resistivity and the porewater electrical resistivity (Archie 1942), are estimated using the equation:

$$\rho_f = F \times \rho_w \quad (2)$$

Where ρ_f is the formation electrical resistivity and ρ_w is the pore water electrical resistivity.

The sediments in the Red River flood plain, with either fresh or salty porewater, will show changes in the formation electrical resistivity, with relatively high resistivities in the freshwater zones and relatively low resistivities in saltwater zones. The transient electromagnetic (TEM) method was used to map the distribution of fresh and salty porewater in the sediments. This method has earlier proved suitable for mapping the depth to and the conductivity of highly conductive layers such as salty water in coastal aquifers (Stewart 1982; Fitterman and Stewart 1986; Mills et al. 1988; McNeill 1990; Spies and Frischknecht 1991; Goldman and Neubauer 1994; Auken et al. 2003; Kafri and Goldman 2005; Nielsen et al. 2007; d'Ozouville et al. 2008). The instrument used was a Protem 47 (Geonics Ltd.,) with a 40 m × 40 m transmitter loop in a central loop configuration. The turn-off time for the transmitter current was 2.5 μs. This relatively short turn-off time, in combination with early time windows, allows for a proper description of the resistivity properties of the uppermost parts of the subsurface. The decay of the secondary magnetic field recorded by the receiver coil was sampled over three segments to handle the high dynamic range of the received signal. For each segment, measurements were made in 20 time windows (gates). Initial noise tests showed that the signal-noise level was very high in the study area. Current levels were between 0.5 and 3 amperes (A) producing a maximum magnetic moment of 4,800 A × m^2.

A total of 170 TEM soundings with acceptable data were conducted in the Red River flood plain in the period from November 2009 to March 2010. The distance between two measurements is typically 2 km in the four survey lines (Fig. 3). Measurements were, if at all possible, avoided at places with risk of coupling from infrastructure such as houses, radio stations and power lines. Dependent on the resistivity structure of the subsurface a minimum distance of 100–200 m was kept between the measuring points and the conductive installations at all times.

The initial TEM data processing, i.e. editing of data and assignment of data uncertainties, was done with the SiTEM software (Auken et al. 2002). Subsequently, the TEM data were inverted profile wise to obtain one-dimensional (1-D) resistivity models of the subsurface using a laterally constrained inversion (LCI) scheme, as described by Auken et al. (2005), (2008). The LCI approach links 1-D resistivity models using a soft constraint on the layer resistivities and layer boundaries. The constraints can be seen as an a priori value for the expected geological variations between soundings.

The data from the geophysical logging and TEM soundings were used to establish an electrical resistivity model of the subsurface sediments and these was subsequently converted to a hydrogeological conceptual model using geological data from groundwater monitoring boreholes. Defined water types (fresh groundwater, salty paleowaters and saltwater from recent intrusions) were finally compared with existing data from chemical inorganic analysis of groundwater samples from boreholes, and maps were constructed with extrapolations of these data from the survey lines.

Results and interpretation

Since the borehole geophysical logging results yield important data and useful insight to be used in the interpretation of the TEM soundings, these data will be presented first. The TEM soundings data will be shown together with geological models displaying the distribution of Holocene and Pleistocene sediments along the four survey lines.

Geophysical borehole logging

The results of the borehole logging in the selected 38 monitoring boreholes can be generalized and displayed with data from four borehole logs as shown in Fig. 4. In Pleistocene and Holocene deposits with fresh groundwater, a positive correlation exists between the sediments' natural gamma radiation readings and the formation electrical conductivity readings. In clays, relatively high gamma radiation and formation electrical conductivity values are observed, whereas in sands low values are recorded (Fig. 4, borehole Q119). This clearly shows that the formation electrical conductivities, and hence electrical resistivities, are primarily controlled by variations in

DOI 10.1007/s10040-012-0874-y

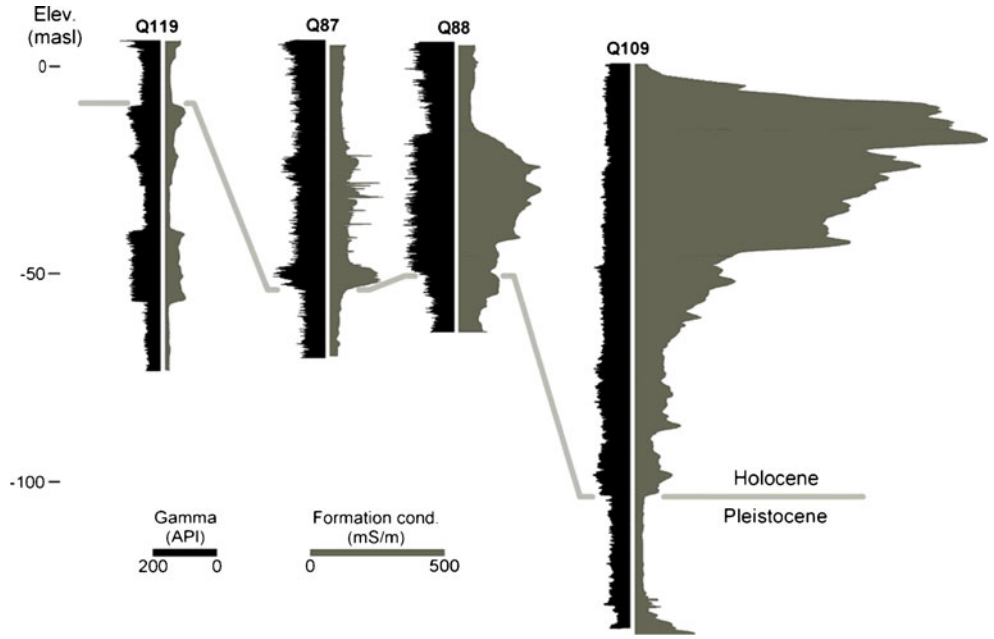

Fig. 4 Selected results from geophysical borehole logging in the national monitoring boreholes. Measured natural gamma radiation data are shown in *black* and measured formation electrical conductivity data are shown in *grey*. For the location of the four boreholes see Fig. 3

lithology and not the water electrical conductivities. In borehole Q119, the natural gamma readings in sands and clays are clearly distinguished, with typically readings in the sands of 40 API (American Petroleum Institute units) and in clays of 60–80 API. The relatively high API reading in the sand is caused by a high content of potassium (K) bearing mica minerals such as muscovite and biotite. The borehole Q119 was drilled in an area with fresh groundwater, 15 km downstream of Hanoi, and the approximately 75-m deep borehole penetrates two fining-upward Pleistocene sedimentary cycles and one Holocene fluvial cycle (Fig. 4). Formation electrical conductivities in the clays with fresh groundwater are between 40 and 60 mS/m, corresponding to formation resistivities between 17 and 25 ohm-m (Eq. 1). The formation resistivities in the sands are between 100 and 150 ohm-m and values up to 200 ohm-m are obtained in gravel layers.

The monitoring boreholes Q87 and Q88 were drilled approximately 60 km from the coastline (Fig. 3), in the intrinsic valley south of the Red River (Fig. 1). Geological information from Q88 shows an upper 25-m-thick fining-upward fluvial Holocene cycle with sands grading upward into clays. The natural gamma measurements support the geological description. Formation electrical conductivities in this cycle are from 30 to 50 mS/m, corresponding to formation resistivities between 20 and 30 ohm-m, indicating a fresh porewater composition in the sediments. A lithology with mainly fine sands and clays is reported from depths between 25 and 55 m, and these must be interpreted as marine sediments filling up the intrinsic valley. High natural gamma radiation in this cycle, with readings up to 125 API, confirms clay-rich deposits in this cycle. Formation electrical conductivity values in the clays show a bell-shaped log patterns with values as high as 320 mS/m (equal to 3 ohm-m) in the central parts and decreasing values towards adjacent layers with low natural gamma radiation (sands). The bell shaped log track in this fairly geologically homogeneous clay layer must be interpreted as reflecting high salinity porewater in the middle of the clay with concentration gradients of total dissolved solids (TDS) in the porewater towards the sandy layers. The poorer correlation between the gamma radiation and formation electrical conductivity in parts of this borehole indicates that the electrical properties in the clay are influenced by the salinity of the porewater, and only indirectly by lithological variations. Lower natural gamma radiation is observed in the underlying Pleistocene sands, and the formation electrical resistivities are 30 ohm-m on average, indicating brackish groundwater in the aquifer at this location.

The monitoring borehole Q87 is located close to borehole Q88 (Fig. 3). The geophysical borehole log for Q87 identifies two sedimentary cycles in the Holocene deposits (Fig. 4), as was the case in borehole Q88. The natural gamma radiation readings in the Holocene marine sediment cycle are lower than those in borehole Q88, indicating more coarse clastic deposits dominated by quartz minerals. The natural gamma readings in Q87 are typically 50 API, except a few layers with values between 70 and 100 API. Observed formation electrical conductivities in the marine sequence in borehole Q87 are typically between 50 and 100 mS/m, corresponding to formation resistivities between 10 and 20 ohm-m. The lower amount of salty groundwater in the marine sediments in this borehole could be interpreted as being the result of a different leaching mechanism in marine sediments of the same age. This question will be addressed in the Discussion section. The concentration of chloride in groundwater sampled from the Pleistocene aquifer in borehole Q87 was 1,560 mg/L, and the water

 DOI 10.1007/s10040-012-0874-y

electrical conductivity values are between 60 and 120 mS/m (Jessen et al. 2008).

The borehole Q109 was drilled 10 km from the coastline, close to a tributary of the Red River (Fig. 3). The geophysical logging results from the upper part of this hole reveal that there is no correlation between the natural gamma radiation of the sediments and formation electrical conductivities, and the conductivities are very high compared to what is seen at other locations in the flood plain. The drillers log from this borehole describes a lithology in the Holocene dominated by mud from the surface at +2 masl to a depth of −100 masl, which must be interpreted as shallow marine deposits. Coarse-grained Pleistocene deposits were encountered below the Holocene deposits and these are overlying Neogene deposits found at −130 masl. The formation electrical conductivities in the upper 15–20 m of the Holocene deposits show values as high as 2,000 mS/m, corresponding to a formation electrical resistivity of 0.5 ohm-m. This distribution of the formation electrical conductivity, with decreasing values with increasing depths in the borehole, suggests that the source of the salty water could be salty bottom water in the adjacent river. The formation electrical conductivity in the Pleistocene aquifer is 25 mS/m, corresponding to a formation electrical resistivity of 40 ohm-m.

Interpreted specific formation resistivities from the borehole logging in the 38 boreholes are shown in Table 1. Based solely on the results from the borehole logging, the flood plain can be divided into three areas, for which geographical extents are indicated in Fig. 3. These areas are:

1. An area with fresh groundwater defined by formation resistivities in the clays between 15 and 25 ohm-m, resistivities in the saturated silt and sand between 25 and 100 ohm-m, and resistivities as high as 200 ohm-m in gravel deposits. The area with fresh groundwater is from the apex of the flood plain to 25 km SE of Hanoi (Fig. 3).
2. An area with medium saline groundwater, mainly demarcated by results of logging in boreholes aligned in 'survey line 2' parallel to the coastline. The geographical extent of this area is from 25 km SE of Hanoi and to 20–40 km from the coastline (Fig. 3). The formation resistivities in the clays in this area are between 3 and 15 ohm-m, and between 15 and 150 ohm-m in the sand/gravel.
3. High saline groundwater has been observed in boreholes at distance up to 35 km from the coastline, where formation resistivities in the clays are between 0.5 and 3 ohm-m, and below 20 ohm-m in the sand/gravel (Table 1).

Results from the TEM soundings

A typical example of the TEM measurements, including noise and signal levels for the three recorded segments of the soundings, is shown in Fig. 5. Generally, the signal response is significantly stronger than the background noise level and only the latest time gates of the high segment are affected by background noise. Low signal-to-noise ratios were only observed in the most northern parts of the plain where uplifted bedrock is present near the surface, and these measurements have been discarded. Five layers for the LCI models were used, and obtained data fit well within the noise levels for all four profiles. The data residuals, normalized to the noise on the data, are stated for the individual LCI sections in Figs. 6, 7, 8 and 9. If the soundings had been inverted as independent soundings, some could have been inverted with only three or four layers, but in the LCI approach, the soundings with the highest complexity defines the number of layers. The geographical location of the profiles with TEM soundings in the four survey lines are indicated in Fig. 3, and the LCI modelling results are given in the Figs. 6, 7, 8 and 9. The TEM sections are all presented with an interpolated image behind the individual sounding results to strengthen the visual interpretation of the soundings.

Table 1 Formation resistivities from borehole logging

Groundwater type	Lithology	Formation resistivity ohm-m
Fresh	Clay	15–25
	Silt/sand	25–100
	Sand/gravel	100–200
Medium saline	Clay	3–15
	Sand/gravel	15–150
High saline	Clay	0.5–3
	Sand/gravel	< 20

Survey line 1

This survey line is located close to Hanoi and is oriented SW–NE (Fig. 3). The length of the geological cross-section in this line is 52 km (Fig. 6a), and the length of the

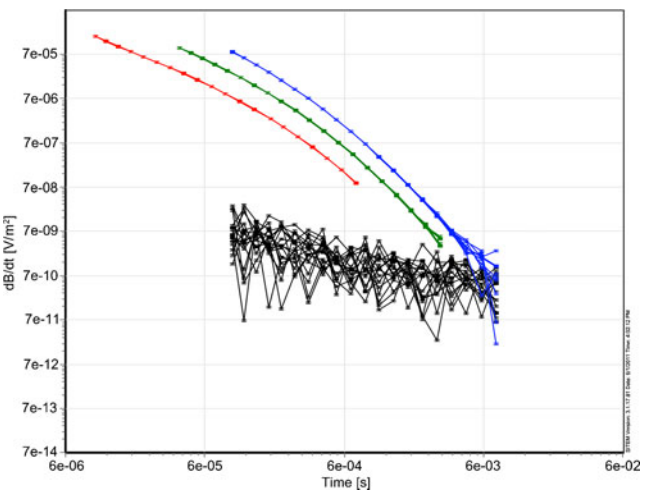

Fig. 5 Typical signal-and-noise-response-time gate measurements in the transient electromagnetic soundings. The *red line* shows the ultra high segments, the *green line* the very high segments and the *blue line* the high segments. Note that measured noise responses shown with *black lines* are lower than the signals excepted for the very last measurements in the high segments

DOI 10.1007/s10040-012-0874-y

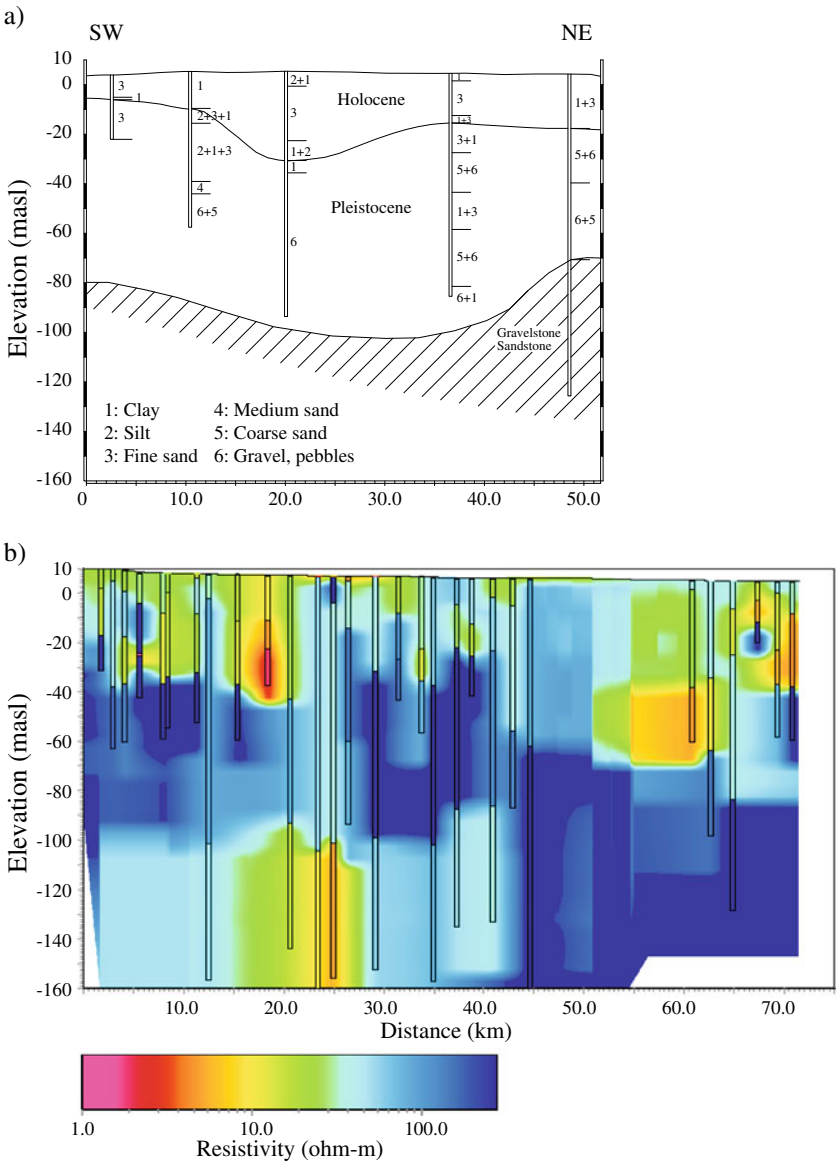

Fig. 6 Survey line 1: **a** Simplified geological cross-section using data from boreholes in the national groundwater monitoring network. For the number codes in the geological logs see the legend. **b** LCI inversion models of measured TEM soundings in the geophysical profile in survey line 1. Formation electrical resistivities in the five layers LCI models are shown in the legend. For the geographical location of survey lines see Fig. 3

adjacent geophysical profile, with LCI models of 30 TEM soundings, is 73 km (Fig. 6b). Geological information from drilling in this area shows a 15–35-m-thick Holocene sequence with fine sand, silt and clay. The coarse-grained sediments must be interpreted as fluvial channel deposits, whereas the more fine-grained sediments were laid down on flood plains also hosting oxbow lake systems. The underlying Pleistocene deposits are present in thicknesses exceeding 80 m, and they are dominated by deposits of cobbles, gravel, sand, silt and clay arranged sequentially in up to three overall fining-upward cycles. Neogene gravel and sandstones have been found in the most NE part of this survey line at depths of 80–90 m, whereas in the central parts, the underlying pre-Quaternary deposits must be lying below a depth of 100 m (Fig. 6a).

The LCI models of the 30 TEM soundings from survey line 1 reveal thick sequences of relatively high resistivity layers (Fig. 6b). The most near surface layers have thicknesses of 1–5 m and model resistivities between 10 and 20 ohm-m. The deeper model layers show resistivities between 20 and 100 ohm-m, and towards the NE and SW, the deepest layer is a high resistivity layer with values as high as 3,000–5,000 ohm-m.

The hydrogeological interpretation of the geological and geophysical data from survey line 1 suggests up to 100-m-thick unconfined and confined freshwater-bearing aquifers in coarse-grained Holocene and Pleistocene deposits. The geological data from drilling and the resistivities of the top layers indicated that clays with freshwater are widespread in this area, and residual

DOI 10.1007/s10040-012-0874-y

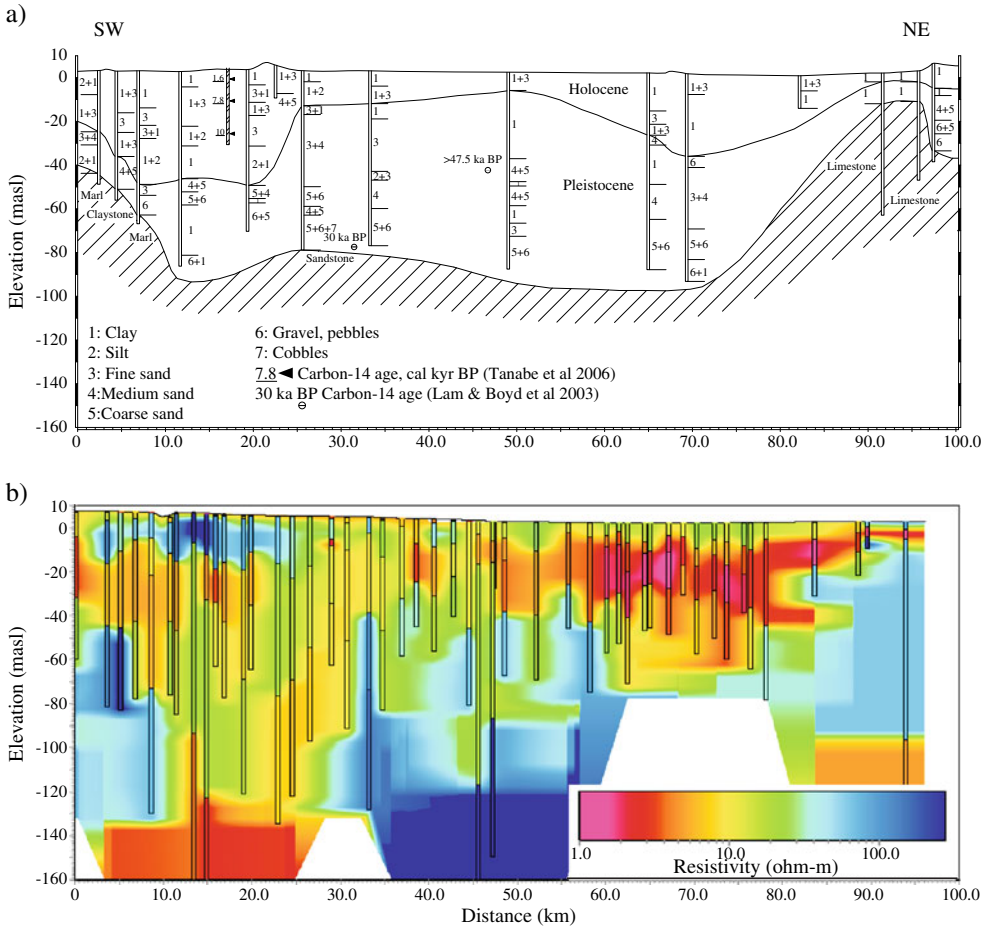

Fig. 7 Survey line 2: **a** Simplified geological cross-section using data from boreholes in the national groundwater monitoring network. **b** LCI inversion models of measured TEM soundings in the geophysical profile in survey line 2

saltwater has been leached out where these layers are marine terraces. The resistivities up to 100 ohm-m in large sections of the survey line suggest that freshwater is present in the sandy aquifers. Both the drilling and TEM models show that up to 10-m-thick layers of clay with silt are present in this otherwise regional sandy aquifer system, but model resistivities of these layers reveal that they are freshwater bearing. The high-resistivity layer at greater depth represents the underlying Neogene consolidated sediments, which might be an aquifer where the sandstone is fractured.

Survey line 2

Survey line 2 is located perpendicular to the known deep intrinsic valley with Holocene sediments, at a distance from the coastline of approximately 60 km (Fig. 3). The length of the geological cross-section in this line is 100 km (Fig. 7a) and the adjacent geophysical profile, with 48 TEM soundings, is 96 km. The resistivity section from the LCI models of the TEM measurements is shown in Fig. 7b.

Geological information from drilling reveals Holocene deposits thickness exceeding 50 m in the intrinsic valley towards the SW. A similar erosion structure, although less deep, can be identified in the NE part of the survey line, where the Holocene deposits are reported in thickness of 30–40 m. The sediments in these two erosion structures are dominated by clays, silts, and fine sands, which at least in the most southern intrinsic valley have been described as marine sediments (Tanabe et al. 2003a). Holocene sediments in thicknesses between 10 and 20 m are present in the central parts of this survey line, dominated by sands and clays which most likely have been deposited during the Holocene transgression (Fig. 7a). Pleistocene deposits are present in thicknesses exceeding 70 m in the central parts of survey line 2, whereas to the SW and NE, erosion has reduced the thickness of these layers (Fig. 7a). The lithology of the upper part of the Pleistocene deposits is in the central part dominated by thick layers of clays and fine sands, which according to Tran et al. (1991) must be interpreted as the upper transgressive part of the uppermost third Pleistocene sedimentary cycle. The Pleistocene deposits below the two erosion structures are dominated by coarse-grained clastic deposits dominated by cobbles, gravel and sand in an overall fining-upward sequence (Fig. 7a). Limestones and claystones deposits are from drillings reported from depths of 50 m in the most SW parts of this line, and limestone has also been reported in the most NE part of the line, from depths of only 10 m. In the central part, sandstone and siltstones can be found at depths of 80–90 m.

DOI 10.1007/s10040-012-0874-y

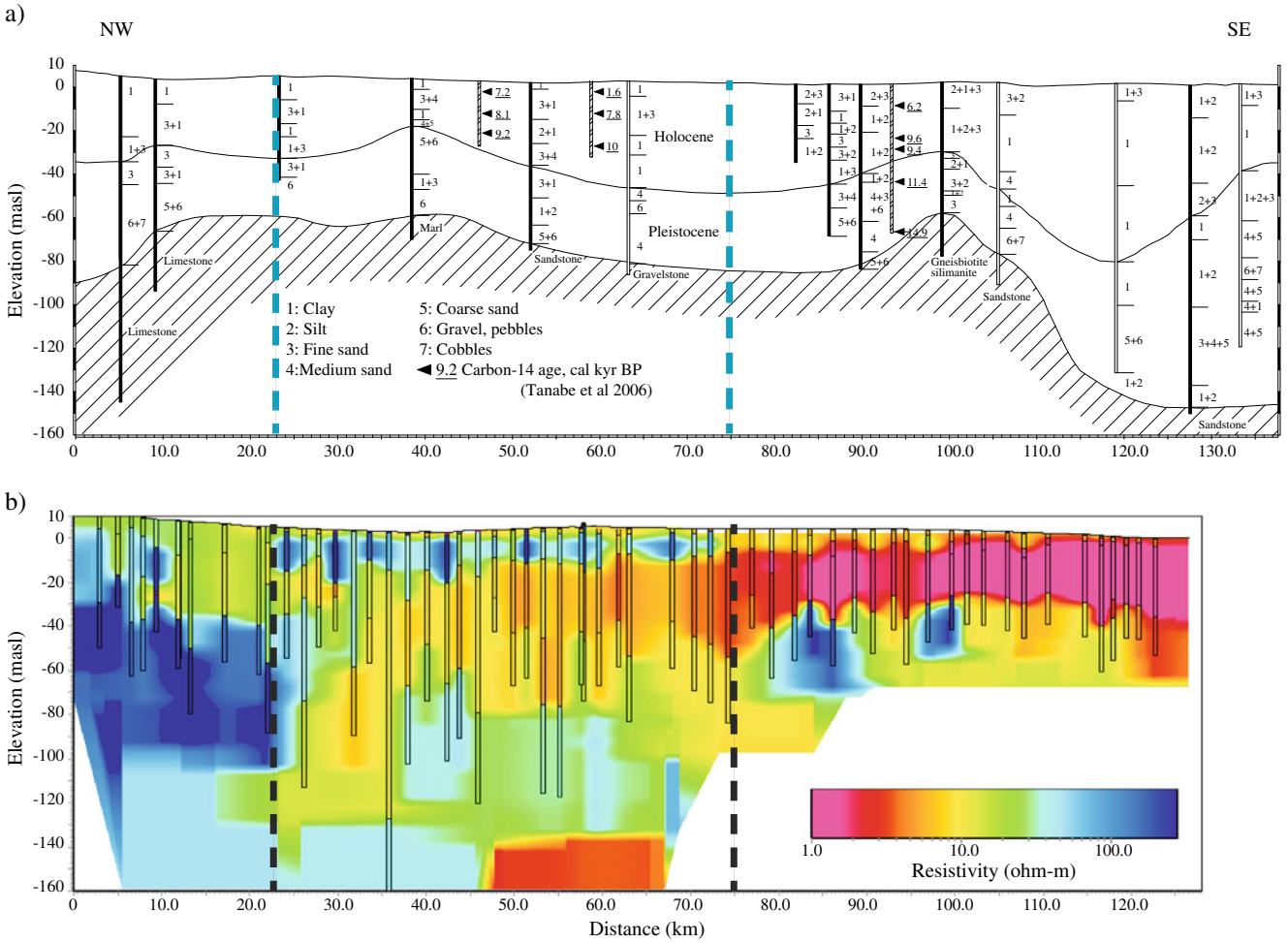

Fig. 8 Survey line 3: **a** Simplified geological cross-section with data from boreholes in the national groundwater monitoring network. **b** LCI inversion models of measured TEM soundings in the geophysical profile in survey line 3. Note that this geophysical profile has been divided into three sub-profiles

The LCI modelled resistivities in the uppermost layers, representing resistivities from the upper 10 m of the Holocene deposits, are in large portions of the sections below 10 ohm-m (Fig. 7b). An exception from this general picture is the shallow parts in the SE intrinsic valley, with resistivity values from 60 to 500 ohm-m. In the intrinsic valleys towards SE are model resistivities as low as 1–10 ohm-m, and similar low resistivity values are also obtained in the LCI models in the valley structure towards the NE (Fig. 7b). Resistivities with values between 5 and 35 ohm-m are obtained in deeper layers; and even higher resistivities, with values up to 250 ohm-m, are presented in the deepest LCI model layer in the central parts (45 km) of the section (Fig. 7b).

The hydrogeological interpretation of the geological and geophysical data from survey line 2 suggests near-surface confining-clay layers with relict salty groundwater in marine terraces. The underlying layers, with resistivities from 100 to 500 ohm-m, must be interpreted as responses from fresh groundwater in sandy deposits with variable saturation, the highest values from unsaturated sands. The very low resistivity layers in the two intrinsic valleys stem from salt porewater in the marine deposits filling up the former valley structures. The variations in salinity of the porewater must be controlled by the leaching processes in the sediments during the approximately 8.5 kyr after their deposition (see section Discussion). The monitoring boreholes Q87 and Q88 are located in this survey line, between 15 and 20 km, and induction logging in these boreholes revealed great variations in the vertical conductivity and, hence, resistivity in these deposits (Fig. 4). The LCI model resistivities in the deeper layers, representing the coarse-grained Pleistocene deposits, show large variations reflecting a variable leaching of salt groundwater from the Holocene deposits to the underlying deposits. Jessen et al. (2008) studied the water composition in the Pleistocene aquifer in most SW parts of survey line 2, and reported concentrations of chloride between 120 and 3,000 mg/L. The high LCI model resistivity layer in the NE parts of the section is interpreted as reflecting the resistivity in the underlying limestone deposits (Fig. 7a).

Survey line 3

Survey line 3 is oriented perpendicular to the coastline in the intrinsic valley south of the Red River (Fig. 3). The

DOI 10.1007/s10040-012-0874-y

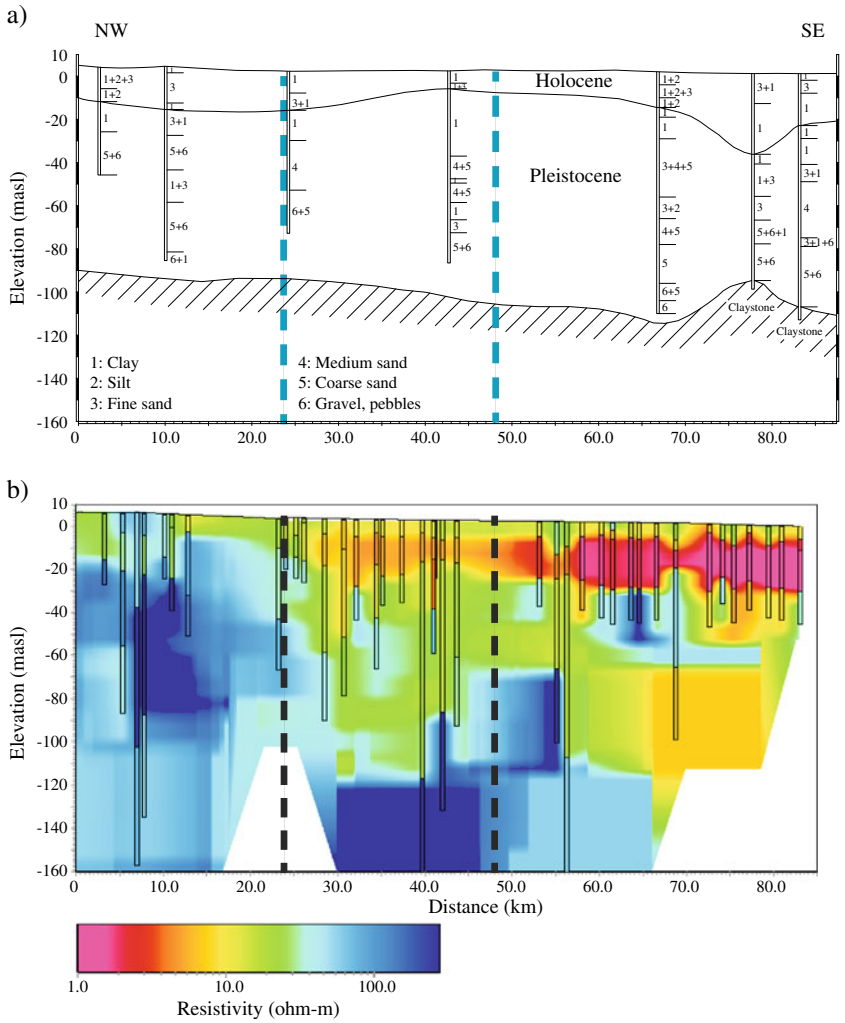

Fig. 9 Survey line 4: **a** Simplified geological cross-section with data from boreholes in the National Groundwater Monitoring Programme. **b** LCI inversion models of measured TEM soundings in the geophysical profile in survey line 4. Note that this geophysical profile has been divided into three sub-profiles

length of the geological cross-section is 135 km (Fig. 8a), and the geophysical profile, with data from 57 TEM soundings, is 128 km. From NW to SE, the resistivity profile is divided into three sections: (1) a landward section from 0 to 23 km; (2) a central section from 23 to 75 km and (3) a coastal section from 75 to 128 km, all of which show characteristic formation resistivity distributions (Fig. 8b).

The geological information from boreholes in this survey line shows a Holocene sequence with a thickness from 30 to 80 m, dominated by fine sand, silt and clay (Fig. 8a). The NW part of this survey line intersects the approximately 20-km-wide intrinsic valley, whereas towards the SE, the line cuts through the buried valley, which is reflected in the observed variations in thickness of the Holocene sediments. The Holocene sediment thickness is up to 80 m in the central parts of the buried valley and only 30–40 m in the flank of the structure (Fig. 8a). The thickness of the Pleistocene deposits towards the NW is up to 50 m, and thicknesses increase towards the coast reaching 120 m. The Pleistocene sediments are composed of cobble, gravel, pebble, sand, silt and mud in overall fining-upward sequences. Drilling has revealed Triassic limestones towards the NW at depths between 65 and 95 m, and an uplifted block with gneiss has been encountered at a depth of 60 m at a distance of 40 km from the present coast line. Near the coast, the Pleistocene deposits are overlying Neogene sandstones at depths of 150 m.

The resistivities of the TEM soundings in the landward section (0–23 km) show increasing LCI model resistivities with increasing depth. Layer resistivities in the upper approximately 10 m are from 10 to 20 ohm-m and a second layer with thickness from 20 to 40 m has resistivities from 20 to 700 ohm-m. The hydrogeological interpretation of the geological and geophysical data in this landward section of survey line 3 resembles closely that of survey line 1. The data indicate a near-surface confining clay layer overlying unsaturated and saturated sand in Holocene and Pleistocene sandy aquifers with freshwater, which again is overlying the limestone formation. There are no indications of salty groundwater in this part of the line.

DOI 10.1007/s10040-012-0874-y

The model of the TEM soundings from the central section of this line (23–75 km) displays a conductive 1–2-m-thick top-layer, with resistivities typically below 10 ohm-m. Underlying this a 10–45 m thick layer with typical resistivity values from 30 to 70 ohm-m and a few intervals with layer values as high as 700 ohm-m. The third and fourth layers in the LCI geophysical models from this section have thickness of 40–50 m and resistivities of 5–10 ohm-m, and the fifth and deepest layer has resistivities of 20–30 ohm-m. The hydrogeological interpretation of the data from this central part of survey line 3 corresponds to the interpretation of the SW part of survey line 2 (Fig. 7b). The data suggest uppermost confining clay layers from marine terraces containing salty porewater, and the second high-resistivity layers represent regional Holocene unconfined and confined aquifers in sandy deposits with freshwater. The lower layers in the geophysical model must be interpreted as representing a deep Pleistocene aquifer with variable concentrations of saltwater. Jessen et al. (2008) report chloride concentrations between 875 and 3,000 mg/L in groundwater samples from Pleistocene aquifers in this part of the Red River flood plain.

The LCI model results of the TEM soundings in the coastal section (75 to 128 km) show predominantly very low resistivities, with typical values of 1–3 ohm-m, from the surface to depths of more than 50 m. The monitoring borehole Q109 (Fig. 4) is located at this survey line (Fig. 3) and geophysical logging in this section of the survey line shows in detail the vertical resistivity profile from the TEM measurements. Isolated near-surface lenses, with high resistivities up to 30–40 ohm-m, are seen in this section with otherwise low resistivity sections. The upper high-conductivity layers in the Holocene sediments are underlain by medium-to-high-resistivity layers, as seen in other parts of this survey line (Fig. 8b). The hydrogeological interpretation of the TEM soundings in this section suggests uppermost confining clays with salty porewater, but areas with fresh shallow groundwater are locally present. Continuous vertical electrode soundings conducted in these areas confirm the presence of shallow freshwater resources in isolated lenses (Lassen 2009). The very low resistivities in the Holocene deposits in this section, compared to what have been observed in the sediments in more inland areas, point to higher concentrations of TDS in the porewater. The obtained formation resistivities in the deep Pleistocene aquifers with variable saltwater composition reflect a variable leaching of salty porewater from the Holocene deposits. The high resistivities in the central part of the section are electrical responses from the up-faulted basement block.

Survey line 4

Survey line 4 is located NE of the Red River perpendicular to the present coastline (Fig. 3). The length of the geological cross-section in this survey line is 87 km (Fig. 9a) and the geophysical profile with 35 TEM soundings is 85 km (Fig. 9b). Based on resistivity variations in the LCI modelling of the TEM soundings, this survey line is also divided into three sections: (1) a landward section from 0 to 24 km, (2) a central section from 24 to 47 km, and (3) a coastal section from 47 to 85 km (Fig. 9b).

Data from the drilled borehole along this survey line show a thickness of the Holocene deposits of 15–20 m in the most inland part and up to 35 m closer towards the coastline, where the underlying Pleistocene deposits have been eroded (Fig. 9a). The lithology of the Holocene deposits is dominated by clays and fine sands. The uppermost Pleistocene layer is, as in survey line 2, a continuous clay layer having a thickness of up to 35 m in the central part of the line and only 10 m towards the SE, where the layer has been eroded and later filled up with Holocene deposits. The lower part of the Pleistocene deposits are coarse-grained deposits of pebbles, gravel and sand with a few thin clay layers, laid down in two or three fining-upward sequences as seen in other parts of the Red River flood plain. Boreholes logs along this line have shown that underlying the Pleistocene layers are Neogene claystones, and these are present from depths of 80 m inland to 100–120 m closer to the coastline.

The results from LCI modelling of the TEM soundings in the most NW section (0–24 km) show that the layers in the upper 30 m are dominated by formation resistivities between 20 and 50 ohm-m, and below this depth, and down to 100 m, the resistivities are higher with values from 50 to 100 ohm-m. The geological and geophysical data of the most NW part of this survey line suggest the presence of a regional freshwater aquifer in Holocene and Pleistocene sandy sediments, with a low resistivity layer (10–20 ohm-m) representing a clay layer.

The models of the TEM soundings in the central part of this survey (24–47 km along the profile) show increasing resistivity with increasing depth. The uppermost 1–10 m has layer resistivities between 10 and 20 ohm-m, and this zone is overlying a 20-m thick zone with resistivities of approximately 5 ohm-m. The deeper layers in the models have a total thickness of 50–60 m and resistivities between 50 and 100 ohm-m. The data from the central parts of this survey line suggest an upper 1–10 m sandy and clay rich unit with freshwater, but salty porewater is also observed in smaller areas, most probably from sediments formed as marine terraces with connate salty porewater. The reported upper Pleistocene clay layer is clearly shown as a low resistivity unit with resistivities that indicate sediments containing residual salty porewater. The relatively high-resistivity model layers in the deeper Pleistocene layers are interpreted as coming from a fresh to brackish groundwater in sandy and more coarse-grained deposits. Jessen et al. (2008) reported groundwater chloride concentration between 400 and 800 mg/L in this part of the Pleistocene aquifer in the flood plain.

The models of the TEM soundings nearest the coastline in survey line 4 (47–85 km along the profile) displays an upper 1–5 m thick layer with variable resistivity, from 5 to 40 ohm-m, overlying a 20–30-m-thick zone with resistivities between 1 and 2 ohm-m. Beneath these layers is a 20–30-m layer of sediments with resistivities between 10 and 30 ohm-m at distances 20 km from the coast and

DOI 10.1007/s10040-012-0874-y

values as low as 3–5 ohm-m closer to the coast. Higher resistivities are obtained in the deepest model layers, with values 40–50 ohm-m towards the NW and 20–30 ohm-m closer to the coast. The hydrogeological interpretation from drilling and modelling of the TEM soundings in this section of survey line 4 has many similarities with the section of survey line 3 that is closest to the shoreline. The layers nearest the surface are clay and sand with freshwater, but they contain lenses of salty groundwater. The underlying low resistivity layers must also here be interpreted as representing salty groundwater in the clay-rich shallow marine sediments. The lowermost low-resistivity layer represents electrical responses from a regional Pleistocene aquifer with clay and fresh or salty water.

The distribution of saline groundwater

With knowledge about the formation factor of the sediments in the Red River delta plain and the relationship between water resistivity and TDS, the results from geophysical data can be used to estimate ranges of groundwater TDS values in the low-permeability layers such as silts and clays. Groundwater TDS values from the high-permeability layers are known from analysis of water samples, the results of which are reported in a national database. Based on this information, maps have been produced to be used in the management of salinity problems in the flood plain. Water types are here named as: fresh groundwater, salty paleowaters and recent saltwater intrusion, with ranges of TDS as defined in the following.

Reported TDS values in areas with fresh groundwater (Postma et al. 2007; Larsen et al. 2008; Jessen et al. 2008; Winkel et al. 2011) are typically below 1 g/L, corresponding to an electrical resistivity below 100 mS/m (ρ_w>10 ohm-m). A TDS below 1 g/L will therefore be used here to separate fresh groundwater from saline groundwater.

Areas in the plain described as having medium salinity from the borehole logging results (Fig. 3), are interpreted as having groundwater influenced by paleosaltwater. The age, or the residence time, of this water still needs to be estimated; the interpretation of the source of the TDS as being from paleowaters is based on the far distance from the sea and on the occurrence dominantly in the low-permeability formations. Assuming a conversion factor of 2, the measured formation conductivities in the clays, of up to 320 mS/m (Fig. 4, borehole Q 88), correspond to water conductivities up to 640 mS/m. Groundwater in these areas shows TDS values up to 15 % of a standard oceanic water composition, i.e. TDS approximately 5 g/L. Groundwater that is here regarded as salty paleowater will therefore be characterized as having a TDS between 1 and 5 g/L.

Water with a TDS above 5 g/L, corresponding to clay formation resistivity below 3 ohm-m (ρ_f>330 mS/m), has been observed in boreholes close to rivers at distances up to 35 km from the coastline (Fig. 3), and in survey lines 3 and 4 in zones up to 35 km from the coastline. This water type is here referred to as water from recent saltwater intrusion, because recent saltwater intrusions along the coastline or from rivers can be the source of the salinity. However, due to the very young age of these sediments of 0.5–1.0 kyr, as given by Tanabe et al. 2006, the higher-salinity porewater (as compared to more inland marine deposits) could also be due to the younger age of these sediments.

The distribution of fresh groundwater, salty paleowater and saltwater in the Holocene and Pleistocene aquifers in the Red River flood plain are depicted in Figs. 10 and 11, respectively. The distribution of the three water types from the geophysical data has been supported with results from chemical analyses of groundwater samples collected from 49 boreholes screened in Holocene aquifers and 244 in Pleistocene aquifers.

Fresh groundwater present in the Holocene aquifers from the mountains in the NW and 25–50 km SE of the capital Hanoi (Fig. 10). The extent of the fresh groundwater zone in the Red River plain is geologically controlled by the extent of the Holocene transgression, and the saltwater leaching mechanism in these sediments. Groundwater with a TDS between 1 and 5 g/L is observed down gradient of the fresh groundwater zone, to about 35 km from the coastline (Fig. 10). In the most NE part of the flood plain, groundwater with a TDS between 1 and 5 g/L is found in the whole coastal region; however, this interpretation is only based on observations from three boreholes. The source of the TDS in the salty paleowater is the marine near-surface terraces and the marine sediments in deeper Holocene valley structures. The leaching process in the shallow aquifers seems to have been more effective in the sediments south of the Red River as compared to the area north of the river, as fresher water is more widespread south of the river. Groundwater with TDS above 5 g/L present in the Holocene flood plain aquifers at the coastline and up to 35 km inland (Fig. 10).

In the high-permeability Pleistocene aquifer, fresh groundwater is present in a larger area than in the Holocene aquifers, mainly due to a faster leaching of salts from these sediments (Fig. 11). Groundwater with TDS between 1 and 5 g/L is observed below the two intrinsic valleys with marine Holocene sediments, and in the coastal areas affected by the saltwater intrusion from rivers (Fig. 11). The observed distribution of TDS in the Pleistocene aquifer is mainly controlled by the downward leaching of dissolved solids from the Holocene deposits above and mixing of water in the high-permeability zones. Small areas with TDS above 5 g/L, observed in the Pleistocene aquifer in the coastal zone, are interpreted as recent saltwater intrusions.

Discussion

The position of the coastline and delta area over geological time has been controlled by a complex dynamic interaction between the rate of sediment supply from the hinterland, the rate of sedimentary basin

DOI 10.1007/s10040-012-0874-y

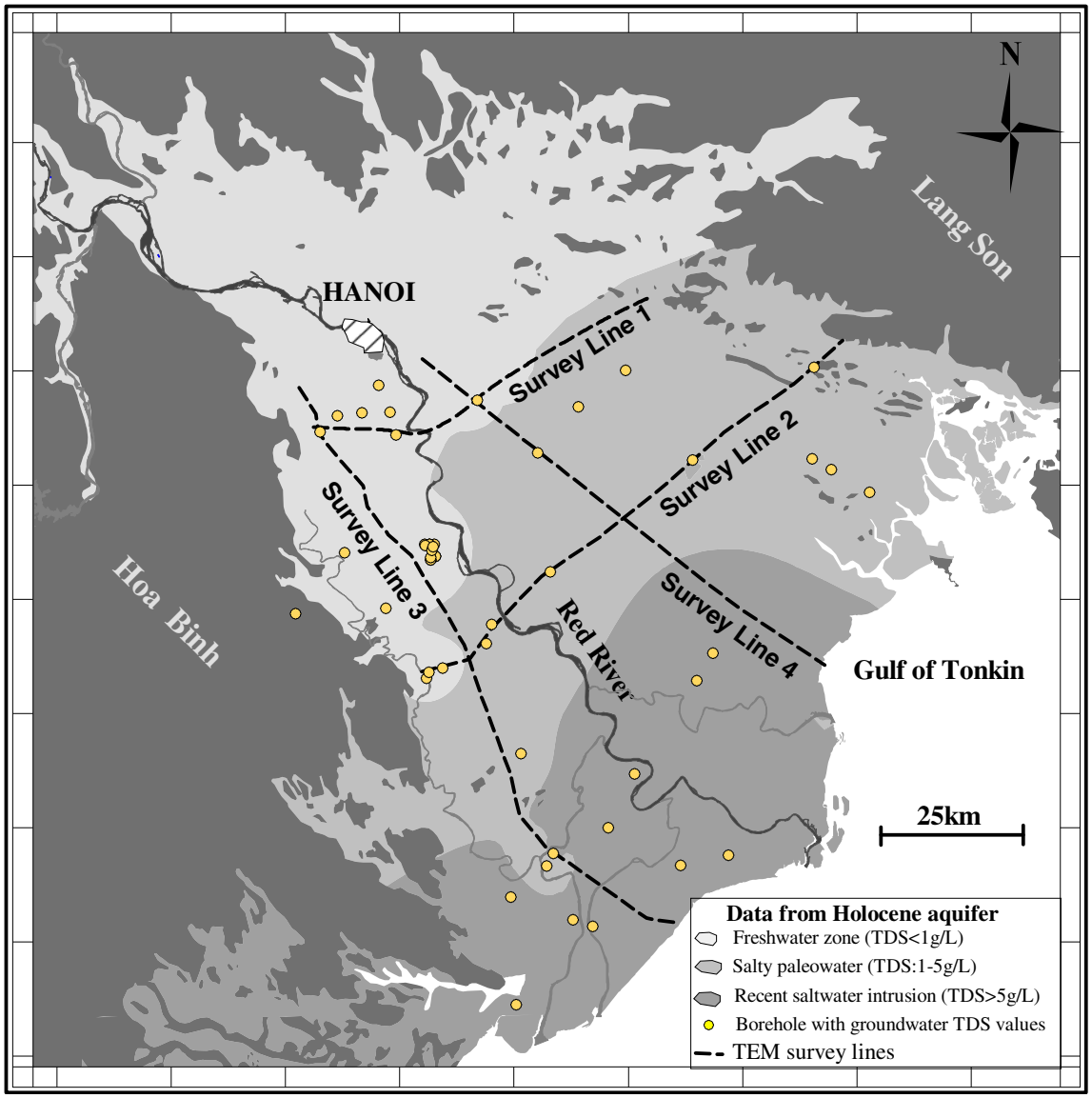

Fig. 10 Map showing areas with fresh groundwater, salty paleowaters and recent saltwater intrusion in Holocene sandy aquifers in the Red River flood plain

subsidence and the rate of eustatic sea-level change (Miall 2000). One of the hydrogeological consequences of changes in the location of the coastal zone is the flushing of marine porewater during regression and saltwater intrusions during transgressions (Edmunds 2001). Sea-level changes during the Quaternary period have varied globally, but a general trend with increasing sea-level of 110–130 m has been seen within the last 20 kyr (Pirazolli 1996). The present-day coastal hydraulic situation must therefore be seen as a period with an exceptional landward migration of the freshwater resources, as the present-day high sea-level stand has only been this high for about 10 % of the last 120 kyr (Edmunds 2001). Freshwater resources were trapped off-shore during low eustatic-sea-level stands (Meisler et al. 1984; Groen et al. 2000; Ruden et al. 2009; Cohen et al. 2010), and old seawater is observed in and below low-permeability formations on-shore (Manheim and Horn 1968; De Vries 1981; Custodio et al. 1987; Bonnesen et al. 2009). The degree of hydraulic disequilibrium, with a given rate in sea-level change, is controlled by the permeability of the near-sea sediments and the slope of the land surface (Kooi et al. 2000).

In the Red River delta flood plain, the recorded 120-m sea-level change in the South China Sea from 20 to 8 kyr (Fig. 2) must have been the overall controlling mechanism of the distribution of fresh and salty groundwater in the Red River plain aquifers. The delta development during the Pleistocene before 20 kyr is more dubious as at least four glacial periods occurred (Dawson 1992). Therefore the marine terraces found more inland that the location of Hanoi must be explained with early and middle Pleistocene transgressions, which reached further inland than the shoreline 9 kyr ago, as suggested by Tanabe et al. 2006 (Fig. 1).

The fast rise of the sea-level after the maximum glaciations 18 kyr ago was completed around 8 kyr ago, followed by an abrupt deceleration in sea-level rise

 DOI 10.1007/s10040-012-0874-y

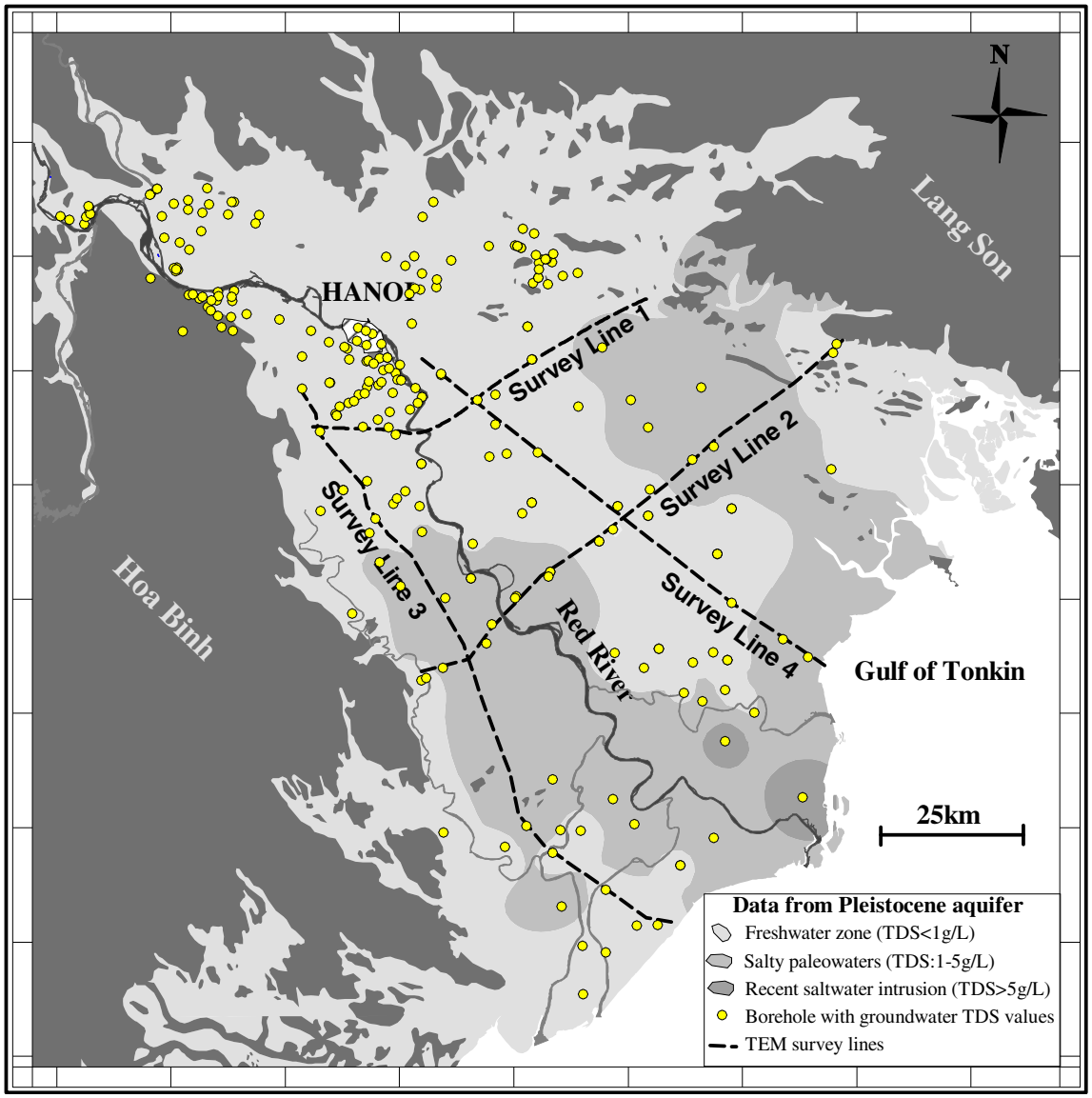

Fig. 11 Map showing areas with fresh groundwater, salty paleowaters and recent saltwater intrusions in Pleistocene sandy aquifers in the Red River flood plain

(Fig. 2). Based on an assessment of 36 deltas worldwide, Stanley and Warne (1994) suggested that this sea-level deceleration initiated delta progradations, which, according to sediment dating, have been documented as initiating between 8.5 and 6.5 kyr. This delta progradation model seems to fit well with observations from the Red River sedimentary basin, where Holocene delta development was initiated approximately 8.5 kyr ago, initially filling up the former Red River valley south of the present Red River (Hori et al. 2004; Tanabe et al. 2003a). This study reveals that an intrinsic valley north of the present Red River was also filled up with marine sediments during the Holocene (Fig. 7a), and geophysical measurements show that salty porewater is still present here (Fig. 7b). Fine-grained sediments from Holocene or late Pleistocene transgressions are present in between these two intrinsic valleys, overlying high-permeability Pleistocene sandy deposits (Fig. 9a).

The transgression during the Holocene, induced by sea-level rise, must have caused an intrusion of seawater into the underlying high-permeability Pleistocene sediments. The rates of the sea-level rises in the South China Sea were 0.25 cm/yr from 20 to 16 kyr and 1.3 cm/yr from 16 to 8 kyr (Fig. 2). Kooi et al. (2000) defined a critical transgression velocity (v_{adv}^{max}, Eq. 3) separating a predominately horizontal from a predominantly vertical saltwater intrusion in high-permeability formations such as the Pleistocene sediments in the Red River flood plain.

$$v_{\mathrm{adv}}^{\max} = \frac{k}{n \times \mu} \times \rho_{\mathrm{s}} \times g \times \tan\beta \tag{3}$$

Where k is the sediment permeability, n is the porosity, μ is the viscosity of the water, ρ_s is the density of the oceanic seawater, g is the gravitational acceleration, and tan β is the tangent of the slope of the land surface.

DOI 10.1007/s10040-012-0874-y

Inserting a rate of sea-level rise of 1.3 cm/yr, a permeability of the Red River Pleistocene deposits of 5×10^{-6} cm^2 (5×10^{-3} m/s), a sand porosity of 25 % and a land-surface slope resembling the present conditions, it can be shown that a predominantly horizontal intrusion of seawater into the Pleistocene deposits must have occurred during the Holocene transgression. Refreshing of the Pleistocene deposits must have commenced during the progradation of the delta sediments 8.5 kyr ago, which eventually lead to the present day hydrogeological setting. An advective seaward transport of introduced salty porewater in the Pleistocene aquifer has occurred during the last approximately 8.5 kyr, and using the same aquifer parameters as in the previous calculation, and a seaward hydraulic gradient of 0.1 %, it can be shown that the salty porewater in the Pleistocene deposits was flushed within 1–2 kyr.

A much slower leaching of salty porewater has occurred in the fine grained, overlying marine Holocene deposits. All other parameters being the same, the downward leaching of saltwater from the Holocene to the Pleistocene deposits will be dominantly controlled by diffusion in the relatively low-permeability formations, whereas density-driven transport takes place in the relatively high-permeability layers. The onset of convective density flows in a field setting, with high-salinity water overlying more freshwater, has been estimated by using the Rayleigh number (Groen et al. 2000):

$$R_a = \frac{(\rho_s - \rho_f) \times g \times k \times H}{\mu \times D_e} \quad (4)$$

Where R_a is the Rayleigh number, ρ_f is the density of freshwater, H is the height of the saltwater column overlying the fresh groundwater and D_e is the effective diffusion of dissolved solids in water. The other parameters are defined with Eq. 3.

When the Rayleigh number exceeds a given value, a density-driven downward flow of salty groundwater will take place and salty groundwater is thereby transported into more permeable layers, where the solutes are transported towards the sea by advective groundwater flow. Using the Rayleigh number as the criteria, Wooding et al. (1997) showed, that in natural systems, density-driven flows will occur when sediment permeability exceeds approximately 10^{-14} m^2 (10^{-7} m/s). Permeabilities in this order will occur in sediments with clay/silt composition, which are the dominant lithologies in shallow marine deposits, as in the Holocene sediments in the Red River flood plain. The observations from borehole logging (Fig. 4, borehole Q87 and Q88) suggest that both convective density flow and diffusive salt transport occur in the Holocene sediments in the Red River flood plain. The relative low gamma radiation in borehole Q87 represents values from a relatively high-permeability formation, whereas Q88 contains more K-rich low-permeability clays. Leaching of salty groundwater by diffusion will occur both to the overlying and underlying high-permeability sand layers.

The inversion of fluid systems, with saltwater overlying freshwater, in coastal aquifer systems has been reported by Radhakrishna (2001); Hiroshiro et al. (2006); Akouvi et al. (2008), and may be more worldwide occurring than previously acknowledged. The reason for this phenomenon is the sea-level changes during the Holocene era, deposition of low-permeability formations (aquitards) with marine porewaters and a subsequently slow diffusion out of the clays (Akouviet al. 2008).

It has been shown that in the Red River and its tributaries, salty bottom water is transported as far inland as 35 km from the South China Sea (Vu 1996; Pham 2004; Hoang et al. 2009). Where the river bottom sediments are highly permeable, this salty bottom water may leak into adjacent aquifers, either as a density-driven flow or as a downward flow controlled by a hydraulic gradient. The rising river stands, up to 6 m during the monsoon period (Larsen et al. 2008; Minh et al. 2010), could also generate such saltwater flow from the rivers into the shallow adjacent aquifers. The very high salinities in the Holocene sediments at distances up to 35 km from the coastline, can, however, also be due to the younger age of these sediments, in which there has been less time to flush the original marine porewater.

Conclusions

Based on the geophysical investigations conducted in this study, supplemented by a review of the existing relevant literature, the following conceptual model has been established regarding the extent and origin of fresh groundwater (TDS <1 g/L), salty paleowater (TDS 1–5 g/L) and recent saltwater intrusion (TDS >5 g/L) in Holocene and Pleistocene aquifers in the Red River flood plain:

1. The geological development of the Red River delta plain in northern Vietnam during the Pleistocene is characterized by three overall fining-upwards sequences, with coarse-grained fluvial deposits overlain by flood plain, lacustrine or marine sediments. In a subsequent period, with low sea levels, fluvial systems eroded two deep structures in these Pleistocene sediments, and the valley systems were filled up with marine sediments during progradation of delta fronts, initiated by a decelerating sea-level rise 8.5 kyr ago. The sedimentation during the late Holocene was dominated by fluvial deposits interbedded with overbank clay-rich deposits; natural sedimentation was later efficiently controlled by construction of dykes along the Red River 1 kyr ago.
2. Fresh groundwater has been identified in the Holocene aquifers in the mountains towards the NW and 25–50 km SE of the capital Hanoi. In the underlying high-permeability Pleistocene aquifers, freshwater is more widespread, due to a faster advective flushing of marine porewater.

DOI 10.1007/s10040-012-0874-y

3. Salty paleowater is found in the Holocene aquifers up to 50 km inland south and 75 km north of the Red River. The source of the dissolved solids in the groundwater is oceanic porewater from the Holocene transgression which formed near-surface marine terraces and deeper marine sediments in two intrinsic valley systems in the Pleistocene sediments. Elevated concentrations of TDS (1–5 g/L) are also present in the Pleistocene aquifer below these intrinsic valleys. The mechanism for the transport of solutes from the Holocene to the underlying Pleistocene must initially have been density-driven transport from relatively high-permeability layers and later mainly a diffusive transport from relatively low-permeability layers.
4. Groundwater with TDS above 5 g/L in the flood plain occurs from the coastline and up to 35 km inland. The source of chloride and other solutes in the Holocene sediments in this region is seawater intrusion from rivers and the sea, or leaching of paleowaters from very young marine sediments. More studies are needed to clarify which of these mechanisms are controlling the occurrence of these very high groundwater salinities.
5. The hydrogeological setting in the Red River flood plain and delta sediments in Vietnam, with an inversed salinity profile, has been created as a consequence of the eustatic sea-level changes during the last 8–9 kyr. These sea-level changes have affected all delta and coastal areas worldwide, and the established conceptual model may thus be applicable to similar coastal aquifers, with a proper incorporation of the local geological environments. Such data are furthermore fundamental for the understanding and future assessment of the impact of projected climate change and sea-level rise on aquifers in vulnerable coastal flood plains.

Acknowledgements This work has been supported by the Danish Development Research Council (DANIDA) as part of a research capacity-building project "Water Resources Research in Vietnam". We would like to express our gratitude to Mrs. Ha T. Nguyen from the Center for Water Resource Planning and Investigation for help in the planning of the field work and for useful discussions. The two technicians Erik V. Clausen and Per Jensen from the Geological Survey of Denmark and Greenland are thanked for their great help in conducting the geophysical borehole-logging programme. Finally we also acknowledge the assistance, discussions and good advice from Søren Jessen during the preparation of this manuscript, and for permission to use borehole logging data from the boreholes Q87 and Q88.

References

Akouvi A, Dray M, Violette S, de Marsily G, Zuppi GM (2008) The sedimentary coastal basin of Togo: example of a multilayered aquifer still influenced by a paleo-seawater intrusion. Hydrogeol J 16:419–436

Antonelli M, Mollema P, Giambastiani K, Bishop K, Caruso L, Minchio A, Pelligrini L, Sabia M, Ulazzi E, Gabbianelli G (2008) Saltwater intrusion in the coastal aquifer of the southern Po Plain. Italy, Hydrogeol J 16:1541–1556

Archie GW (1942) The electrical resistivity log as an aid in determining some reservoir characteristics. Trans Am Inst Min Metal Eng 146:54–62

Auken E, Nebel L, Sørensen K, Breiner M, Pellerin L, Christensen NB (2002) EMMA: a geophysical training and education tool for electromagnetic modeling and analysis. J Environ Eng Geophys 7:57–68

Auken E, Jørgensen F, Sørensen K (2003) Large-scale TEM investigation for groundwater. Explor Geophys 34:188–194

Auken E, Christiansen AV, Jacobsen BH, Foged N, Sørensen KI (2005) Piecewise 1D laterally constrained inversion of resistivity data. Geophys Prospect 53:497–506

Auken E, Christiansen AV, Jacobsen L, Sørensen KI (2008) A resolution study of buried valleys using laterally constrained inversion of TEM data. J Appl Geophys 65:10–20

Balia R, Gavaudo E, Ardua F, Ghiglieri G (2003) Geophysical approach to environmental study of a coastal plain. Geophysics 68(5):1446–1459

Barlow P, Reichard EG (2010) Saltwater intrusion in coastal regions of North America. Hydrogeol J 18:247–260

Berg M, Tran HC, Nguyen TC, Viet PH, Schertenleib R, Giger W (2001) Arsenic contamination of groundwater and drinking water in Vietnam: a human health threat. Environ Sci Tech 35:2621–2626

Bocanegra E, Silva GCD, Custodio E, Manzona M, Montenegro S (2010) State of knowledge of coastal aquifers management in South America. Hydrogeol J 18:261–267

Bonnesen EP, Larsen F, Sonnenborg TO, Klitten K, Stemmerik L (2009) Deep saltwater in Chalk of North-West Europe: origin, interface characteristics and development over geological time. Hydrogeol J 17:1643–1663

Buckley DK, Hinsby K, Manzano M (2001) Application of geophysical borehole logging techniques to examine coastal aquifer paleohydrogeology. In: Paleowaters in coastal Europe: evolution of groundwater since the late Pleistocene. Geol Soc Spec Publ 189:251–270

Cheng JM, Chen CX (2001) Three-dimensional modeling of density-dependent saltwater intrusion in multilayered coastal aquifers in Jahe River Basin, Shandong province, China. Groundwater 39(1):137–143

Cohen D, Person M, Wang P, Gable CW, Hutchinson D, Marksamer A, Dugan B, Kooi H, Groen K, Lizarralde D, Evans RL, Day-Lewis FD, Lane JW (2010) Origin and extent of Fresh Paleowaters on the Atlantic Continental Shelf, USA. Groundwater 48(1):143–158

Custodio E (2010) Costal aquifers of Europe: an overview. Hydrogeol J 18:269–280

Custodio EG, Bruggeman GA, Cotecchia V (1987) Groundwater problems in coastal areas. Studies and Reports in Hydrology 35, UNESCO, Paris, p 650

Dawson AG (1992) Ice age earth. Late quaternary geology and climate. Routledge, London, p 293

De Vries JJ (1981) Fresh and saltwater in the Dutch coastal area in relation to geomorphological evolution. In: AJ Loon (ed) Quaternary geology: a farewell to A. J. Wiggers. Geol Mijnbouw 60:363–368

d'Ozouville N, Auken E, Sørensen KI, Violette S, Marsily GD, Deffontaines B, Merlen G (2008) Extensive perched aquifer and structural implications revealed by 3D resistivity mapping in a Galapagos volcano: Earth Planet Sci Lett 269:518–522

Edmunds WM (2001) Paleowater in European coastal aquifers –the goals and main conclusions of the PALAEAUX project. In: Edmunds WM, Milne CJ (eds) Paleowaters in Coastal Europe: evolution of groundwater since the late Pleistocene. Geol Soc Spec Publ 189:1–16

Edmunds WM, Milne CJ (2001) Paleowaters in Coastal Europe: evolution of groundwater since the late Pleistocene. Geol Soc Spec Publ 189

Fitterman DV, Stewart MT (1986) Transient electromagnetic sounding for groundwater. Geophysics 51:995–1005

Funabiki S, Nguyen VQ, Viet PH, Dinh HT (2007) Holocene delta plain development in the Song Hong (Red River) delta, Vietnam. J Asian Earth Sci 30:518–529

General Statics Office (2011) Statistical Handbook of Vietnam. General Statics Office, Hanoi. Available via http://www.gso.gov.vn. Accessed April 24th 2012
Goldman M, Neubauer FM (1994) Groundwater exploration using integrated geophysical technique. Surv Geophys, 15:331–361. Kluwer, Dordrecht, The Netherlands
Gossel W, Sefelnasr A, Wysick P (2010) Modelling of paleo-saltwater intrusion in the northern part of the Nubian Aquifer System, Northeast Africa. Hydrogeol J 18:1447–1463
Groen J, Velstra J, Meesters AGCA (2000) Salinization processes in paleowaters in coastal sediments of Suriname: evidence from δ^{37} Cl analysis and diffusion modeling. J Hydrol 234:1–20
Hiroshiro Y, Jinno K, Berndtsson R (2006) Hydrochemical properties of a salinity-affected coastal aquifer in western Japan. Hydrol Proc 20:1425–1435
Hoang NK, Dang TQ, Hoang TD, Le DK, Nguyen NM, Nguyen TC (1998) Geology and Hydrogeology map of Bac Bo Plain. Scale 1:200,000. Northern Hydrogeology and Engineering Division, Hanoi
Hoang VH, Lassen R, Tran VL, Vu VH, Tran TL, Pham QN, Larsen F (2009) Mapping of fresh and saline groundwater in coastal aquifers in the Nam Dinh Province (Vietnam) by electrical and electromagnetic soundings. APOAMM, The First Asia-Pacific Coastal Aquifer Management Meeting: Mapping for Synergy in the Twenty-first century. Bangkok, 9–11 December 2009
Hori K, Tanabe S, Saito Y, Haruvama S, Nguyen V, Kitamura A (2004) Delta initiation and Holocene sea-level change: example from the Song Hong (Red River) delta, Vietnam. Sediment Geol 164:237–249
Jessen S, Larsen F, Postma D, Viet PH, Ha NT, Nhan PQ, Nhan DD, Duc MT, Nguyen TMH, Trieu DH, Tran TL, Dang HH, Jakobsen R (2008) Paleo-hydrogeological control on groundwater as levels in the Red River delta, Vietnam. Appl Geochem 23:3116–3126
Kafri U, Goldman M (2005) The use of the time domain electromagnetic method to delineate saline groundwater in granular and carbonate aquifers and to evaluate their porosity. J Appl Geophys 57:167–178
Khalil M (2006) Geoelectric resistivity soundings for delineating saltwater intrusion in the Abu Zenima area, West Sinai, Egypt. J Geophys Eng 243–251
Kooi H, Groen J, Leijnse A (2000) Modes of seawater intrusion during transgressions. Water Res Res 36(12):3581–3589
Lam DD, Boyd WE (2003) Holocene costal stratigraphy and the sedimentary development of the Hai Phong area of the Bac Bo plain (Red River delta). Vietnam Aust Geogr 34:177–194
Larsen F, Pham NQ, Dang ND, Postma D, Jessen S, Pham VH, Nguyen TB, Trieu HD, Tran LT, Nguyen H, Chambon J, Nguyen HV, Ha DH, Hue NT, Duc MT, Refsgaard JC (2008) Controlling geological and hydrogeological processes in an arsenic contaminated aquifer on the Red River flood plain. Vietnam Appl Geochem 23(11):3099–3115
Lassen RN (2009) A geophysical and hydrogeological survey of the saltwater intrusion in the Holocene sediments near Nam Dinh in Red River delta, Vietnam. MSc Thesis, Institute of Geography and Geology, University of Copenhagen, Denmark, 103 pp. Available via http://vietas.er.dtu.dk. Accessed 15 Feb 2011
Le JY, Song SH (2007) Groundwater chemistry and ionic ratios in a western coastal aquifer of Buan, Korea: implications for seawater intrusion. Geosci J 11(3):259–270
Lozano E, Coleto C, Manzano M, Custodio E (2002) Saline waters in a coastal area of the National Park of Doñana (SW of Spain) in absence of saline water intrusion. 17th Saltwater Intrusion Meeting, The Netherlands, 6–10 May 2002
Manheim FT, Horn MK (1968) Composition of deeper subsurface waters along the Atlantic continental margin. Southeast Geol 9:215–236
Mathers S, Zalasiewicz J (1999) Holocene sedimentary architecture of the Red River Delta, Vietnam. J Coast Res 15:314–325
Mathers SJ, Davis J, McDonald A, Zalasiewitz JA, Marsh S (1996) The Red River Delta of Vietnam. Technical report WC/96/02, British Geological Survey, Keyworth, UK, p 41
McNeill JD (1990) Use of electromagnetic methods for groundwater studies. In: Ward SH (ed) Geotechnical and environmental geophysics, vol 2. Society of Exploration Geophysicists, Tulsa, OK, pp 191–218
Meisler H, Leahy PP, Knobler L (1984) Effect of Eustatic sea-level changes on saltwater–freshwater relations in the Northern Atlantic Coastal Plain. US Geol Surv Water Suppl Pap 2255
Miall AD (2000) Principles of sedimentary basin analysis. 3rd edn, updated and enlarged, Springer, Heidelberg, p 616
Mills T, Hoekstra P, Blohm M, Evans L (1988) Time-domain electromagnetic soundings for mapping sea-water intrusion in Monterey County, California. Groundwater 26:771–782
Minh LT, Josette G, Gilles B, Didier O, Julien N, Quynh LTP, Thai THT, Anh LL (2010) Hydrological regime and water budget for the Red River delta (northern Vietnam). J Asian Earth Sci 37:219–228
Nguyen TH (2005) Groundwater chemistry and its behavior in Quaternary sediments and possibility for water supply in Northern Plain, Vietnam. PhD Thesis, Hanoi University of Mining and Geology, Vietnam, 159 pp
Nielsen LH, Mathiesen A, Bidstrup T, Vejbæk OV, Dien DT, Tiem PV (1999) Modelling of hydrocarbon generation in the Cenozoic Song Hong Basin, Vietnam: a highly prospective basin. J Asian Earth Sci 17:269–294
Nielsen L, Jørgensen NO, Gelting P (2007) Mapping of the freshwater lens in a coastal aquifer on the Keta Barrier (Ghana) by transient electromagnetic soundings. J Appl Geophys 62:1–15
Pham QN (2000) Groundwater reserves in Red River delta plain and its sustainable development. PhD Thesis, Hanoi University of Mining and Geology, Vietnam, p 144
Pham QS (2004) Study of development of Red River: That Binh River estuaries on the basis of Remote Sensing's Information and GIS for rational exploitation of use of territory (in Vietnamese). PhD Thesis, National University, Vietnam, p 155
Pirazolli PA (1996) Sea-level changes: the last 20,0000 years. Wiley, Chichester, UK, p 211
Post VEA, Kooi H (2003) Rates of salinization by free convection in high-permeability sediments: insights from numerical modeling and application to the Dutch coastal area. Hydrogeol J 11(5):549–559
Post VEA, van der Plicht H, Meijer HAJ (2003) The origin of brackish and saline groundwater in the coastal area of the Netherlands. Neth J Geosci/Geol Mijnb 82:131–145
Postma D, Larsen F, Hue NTM, Duc MT, Viet PH, Nhan PQ, Jessen S (2007) Arsenic in groundwater of the Red River floodplain, Vietnam: controlling geochemical processes and reactive transport modeling. Geochim Cosmochim Acta 71:5054–5071
Radhakrishna I (2001) Saline freshwater interface structure in Mahanadi delta region, Orissa, India. Environ Geol 40(3):369–380
Rangin C, Klein M, Roques D, Le Pichon X, Trong VL (1995) The Red River fault system in the Tonkin Gulf, Vietnam. Tectonophysics 243:209–222
Ruden F, Ammundsen H, Johansen S, Ellingrud S, Abelsen R (2009) Freshwater entrapment in the offshore West Zanzibar Bain. Int. Symposium on Efficient Groundwater Resource Management, Bangkok, 16–21 February 2009
Schimanski A, Stattegger K (2005) Deglacial and Holocene evolution of the Vietnam shelf: stratigraphy, sediments and sea-level change. Mar Geol 214:365–387
Spies BR, Frischknecht FC (1991) Electromagnetic sounding. In: Nabighian MN (ed) Electromagnetic methods in applied geophysics, vol. 2. Society of Exploration Geophysicists, Tulsa, OK, pp 398–402
Stanley DJ, Warne A (1994) Worldwide initiation of Holocene marine deltas by deceleration of sea-level rise. Science 265:228–231
Stewart MT (1982) Evaluation of electromagnetic methods for rapid mapping of saltwater interfaces in coastal aquifers. Ground Water 20:583–545
Steyl G, Dennis I (2010) Review of coastal-area aquifers in Africa. Hydrogeol J 18:217–225

Tanabe S, Hori K, Saito Y, Haruyama S, Le QD, Sato Y, Hiraide S (2003a) Sedimentary facies and radiocarbon dates of the Nam Dinh-1 core from the Song Hong (Red River) delta, Vietnam. J Asian Earth Sci 21:503–513

Tanabe S, Hori K, Saito Y, Haruyama S, Van PV, Kitamura A (2003b) Song Hong (Red River) delta evolution related to millennium-scale Holocene sea-level changes. Quat Sci Rev 22:2345–2361

Tanabe S, Saito Y, Quang LV, Hanebuth TJJ, Quang LN, Kitamura A (2006) Holocene evolution of the Song Hong (Red River) delta system, northern Vietnam. Sediment Geol 187:29–61

Tran N, Ngo QT, Do TVT, Nguyen DM, Nguyen VV (1991) Quaternary sedimentation of the principal deltas of Vietnam. J SE Asian Earth Sci 6:103–110

Vu TC (1996) Salinity Intrusion in the Red River delta. Seminar on Env. and Development in Vietnam, Canberra, 6–7 December 1996. Available via http://coombs.anu.edu.au/~vern/env_dev/papers/pap08.html. Accessed 24 April 2012

Werner AD (2010) A review of seawater intrusion and its management in Australia. Hydrogeol J 18:281–285

White I, Falkland T (2010) Management of freshwater lenses on small Pacific islands. Hydrogeol J 18:227–246

Winkel LE, Trang PTK, Lan VM, Stengel C, Amini M, Ha NT, Viet PH, Berg M (2011) Arsenic pollution of groundwater in Vietnam exacerbated by deep aquifer exploitation for more than a century. PNAS Early Edition 1–6, PNAS, Washington, DC

Wooding RA, Tyler SW, White I (1997) Convection in groundwater below an evaporating salt lake: 1. onset of instability. Water Res Res 33(6):1199–1217

Zengcui H, Yaqin S (1989) Saltwater Intrusion and the countermeasures in some coastal cities in China. China Ocean Eng 3 (2):177–193

Zhang Q, Volker RE, Lockington DA (2004) Numerical investigation of seawater intrusion at Gooburrum, Bundaberg, Queensland, Australia. Hydrogeol J 1:674–687

 DOI 10.1007/s10040-012-0874-y